Particle acceleration and non-thermal emission in Pulsar Wind Nebulae from relativistic MHD simulations

Journal of Physics: Conference Series **642** (2015) 012019 doi:10.1088/1742-6596/642/1/012019

Particle acceleration and non-thermal emission in Pulsar Wind Nebulae from relativistic MHD simulations

B Olmi[1,2,3], L Del Zanna[1,2,3], E Amato[2], N Bucciantini[2,3] and R Bandiera[2]

[1] Dipartimento di Fisica e Astronomia, Università degli Studi di Firenze, Via G. Sansone 1, 50019 Sesto F. no (Firenze), Italy

[2] INAF - Osservatorio Astrofisico di Arcetri, Largo E. Fermi 5, 50125 Firenze, Italy

[3] INFN - Sezione di Firenze, Via G. Sansone 1, 50019 Sesto F. no (Firenze), Italy

E-mail: barbara.olmi@unifi.it

Abstract. Pulsar wind nebulae are among the most powerful particle accelerators in the Galaxy with acceleration efficiencies that reach up to 30% and maximum particle energies in the PeV range. In recent years relativistic axisymmetric MHD models have proven to be excellent tools for describing the physics of such objects, and particularly successful at explaining their high energy morphology, down to very fine details. Nevertheless, some important aspects of the physics of PWNe are still obscure: the mechanism(s) responsible for the acceleration of particles of all energies is (are) still unclear, and the origin of the lowest energy (radio emitting) particles is most mysterious. The correct interpretation of the origin of radio emitting particles is of fundamental importance, as this holds information about the amount of pair production in the pulsar magnetosphere, and hence on the role of pulsars as antimatter factories. On the other hand, the long lifetimes of these particles against synchrotron losses, allows them to travel far from their injection location, making their acceleration site difficult to constrain. As far as the highest energy (X and gamma-ray emitting) particles are concerned, their acceleration is commonly believed to occur at the pulsar wind termination shock. But since the upstream flow is thought to have non-uniform properties along the shock surface, important constraints on the acceleration mechanism(s) could come from exact knowledge of the location and flow properties where particles are being accelerated. We investigate in detail both topics by means of 2D numerical MHD simulations. Different assumptions on the origin of radio particles and more generally on the injection sites of all particles are considered, and the corresponding emission properties are computed. We discuss the physical constraints that can be inferred from comparison of the synthetic emission properties against multiwavelength observations of the PWN class prototype, the Crab Nebula.

1. Introduction

PWNe are a particular class of supernova remnants, born in the violent death of a massive star ($M \gtrsim 8\ M_{\odot}$). The nucleus of the progenitor star gives rise to a highly magnetised, rapidly rotating neutron star, often observed as a pulsar, that emits a magnetised relativistic outflow, the so called Pulsar Wind (PW). Effective confinement of the PW by the slowly expanding debris of the explosion induces the formation of a Termination Shock (TS), at which the flow is slowed down and heated. The Pulsar Wind Nebula arises downstream of this shock as non-thermal emission of the shocked material.

The overall picture can be compared with the solar wind scenario. Even if the nature of the wind is very different in the two cases, both the solar wind and the PW are slowed down at a termination shock, in order to reconnect with the physical conditions of the external medium. The solar wind is a thermally driven outflow, mainly composed of electrons and protons, escaped from the hot solar corona. The PW, instead, is electromagnetically driven and mainly made of electrons and positrons. These are created in the pulsar magnetosphere, where the electrons extracted from the star by the strong electric field present

at its surface, interact with photons and develop a pair cascade. Particles and fields leave then the star vicinity in the form of an outflow whose structure is that of a Parker spiral. The region beyond the PW TS, that is the PWN, can be thought analogous to the Sun's helio-sheath. Its outer boundary is the PWN contact discontinuity, where the bubble of relativistic plasma meets the cold supernova ejecta. This is in turn analogous to the heliopause, where the heliospheric plasma meets the interstellar medium.

PWNe are interesting objects from several different points of view. The first obvious reason is that they enclose the most of the pulsar spin-down energy (in the sense that most of the MHD energy released in the pulsar spin down process is deposited in the nebula in the form of Poynting flux and energetic particles), and so they are the perfect place to look at in order to investigate open questions in pulsar physics.

Moreover pulsars have an important role as galactic antimatter factories, and the knowledge of the exact amount of pair production in their magnetospheres can be fundamental in understanding the cosmic ray positron excess measured by PAMELA and AMS02 [1, 2]. The fact that they are so close and bright makes them a perfect place for studying the physics of relativistic magnetized plasmas.

PWNe are also extremely interesting from the point if view of particle acceleration, together with Supernova remnants they are the most powerful accelerators in the Galaxy. While Supernova Remnants are thought to be the primary sources of hadronic cosmic rays in the Galaxy, in PWNe we have direct evidence of the presence of electrons with PeV energies (the highest energy observed in Cosmic rays of Galactic origin). The acceleration of these particles is likely associated with the presence of a magnetised relativistic shock, an environment where acceleration is most difficult to understand, and the acceleration mechanism at work still represents a deep mystery.

2. PWN observations

PWNe show common observational features: a center-filled emission morphology, flat radio spectra and very broad band non thermal emission, usually extending from radio frequencies to X-rays or even γ-rays [3].

The prototype of the class is the Crab Nebula, one of the best studied objects in the sky, and the one from which we have learnt most of what we know about PWNe [4]. The Crab Nebula shows a very broad band spectrum, with primary emission extending from radio frequencies to $\nu \sim 10^{22}$ Hz, due to synchrotron radiation produced by relativistic particles interacting with the intense ($\sim 100 B_{\rm ISM}$) and highly ordered magnetic field of the nebula. At higher energies (up to $\nu \sim 10^{28}$ Hz), the emission is produced via the Inverse Compton scattering process, between electrons and different target photon fields. The most important of these are photons produced by synchrotron emission, photons from the Cosmic Microwave Background and thermal photons emitted by warm dust. Dust, in the form of silicates and graphite at $T \simeq 40-50$ K, is a common left over of SN explosions, and in the Crab Nebula its thermal emission produces a 'bump' in the spectrum at infrared frequencies.

In the last decade, the *Chandra* X-ray observatory has allowed us to observe the high energy emission properties of PWNe with great details. A very puzzling jet-torus morphology was seen in the Crab Nebula and some other PWNe. The presence of polar jets was the most intriguing feature, since they appeared to originate so close to the pulsar location that collimation upstream of the TS seemed to be required. The best candidate mechanism for jet collimation in PWNe appeared to be magnetic collimation, but this can be shown to be very inefficient in ultrarelativistic flows, such as the flow upstream of the TS is.

Thanks to *Chandra* also many different bright and variable features were found, as *knots* and *rings* in the inner region of the nebula [5].

3. The Pulsar Wind

PWNe are powered by the spin-down of young neutron stars that lose their energy in the form of a wind. From pulsar models we know that the wind must be mainly made of electron-positron pairs and magnetically dominated in the close magnetosphere, within the light cylinder of the star. Thus, defining

the wind magnetization as the ratio between the Poynting flux and the ram pressure of the wind

$$\sigma = \frac{B^2}{4\pi n m_e \Gamma^2 c^2} \tag{1}$$

with n is the comoving particle density, m_e the electron mass, Γ the wind Lorentz factor and c the speed of light, we expect that $\sigma \gg 1$ for $r \sim r_{\rm LC}$.

Beyond the light cylinder the streamlines of the outflow become asymptotically radial and the magnetic field becomes predominantly toroidal. This structure is described by the analytical split monopole model [6], which shows an excellent agreement with numerical simulations [7]. The energy flux has an anisotropic distribution in the wind, with $F \propto \sin^2\theta$, where θ is the polar angle, measured from the pulsar rotation axis. In the equatorial plane the split monopole solution implies a sharp change of polarity in the magnetic field, and thus the presence of a current sheet. This current layer would be infinitely thin in the case of an aligned rotator (magnetic axis parallel to rotation axis), but in general pulsars are not aligned, and the wind structure is more complicated. The inclination between the rotational and magnetic axis of the pulsar leads to a 'ballerina skirt' structure: the current sheet oscillates around the equatorial plane within a region of angular extent equal to the inclination angle. Neighbouring stripes of opposite polarities offer the perfect location for magnetic dissipation to occur [8], and hence σ is likely to decrease with increasing distance from the pulsar in some range of latitudes around the equator.

Indeed, a long standing problem in PWN physics is the so called σ *problem*. As we previously mentioned, near the light cylinder the wind is expected to be magnetically dominated ($\sigma \gg 1$). However, effective deceleration of the flow at the TS is only possible if its magnetisation is not too high. In particular, steady state MHD models in 1 or 2 D [9, 10], pointed to $\sigma \sim v_N/c$ at the TS, with $v_N \approx 10^3 {\rm km}/s$ the expansion velocity of the nebula. This requirement has somewhat been revised and made less severe by later multi-D MHD simulations [11, 12], but considerable dissipation still appears to be required.

As a distinct contrast there is no σ *problem* in solar wind physics. Since the solar wind is thermally driven, its magnetic energy is nowhere dominant, contrary to what happens at the very basis of the Pulsar Wind.

The split monopole wind structure and its use in multi-D MHD simulations provided a straightforward solution to another puzzle in PWN physics that we already mentioned, namely the jet-torus morphology of the high energy emission from these objects. The anisotropic distribution of the wind energy flux produces an oblate TS, more distant from the pulsar at the equator than along the polar axis, where cusps develop. Therefore, the polar jet, in spite of being seen from very close to the pulsar, originates in fact in the downstream region. Here, as shown in many different simulations [13, 11, 14], magnetic hoop stresses can lead to effective collimation. Even if $\sigma < 1$, compression of the toroidal magnetic field downstream of the TS can bring the field up to the equipartition value. When this happens, the magnetic tension diverts the flow towards the polar axis at intermediate latitudes, collimating the polar outflow into a jet. Of course this process only works if σ is sufficiently large: for the parameters appropriate to describe the crab Nebula, 2D simulations indicate $\sigma > 0.01$.

State of the art 3D simulations seem to indicate that in the Crab Nebula the wind magnetization might be σ = a few, with considerable dissipation taking place downstream of the shock. These findings are however preliminary. 3D simulations only extend to few hundred years after the explosion and extrapolation of their results to the actual age of the nebula seem to indicate that the final strength of the nebular magnetic field might be too low and incompatible with the emission spectrum, suggesting that even higher values of the wind σ might be required. The bottom line is that in order to explain the presence of a jet with the observed properties the pulsar wind magnetization must be likely much larger than 0.001 for most of the flow. As we will discuss later, this lower limit on σ is problematic from the point of view of understanding particle acceleration at the termination shock.

4. Numerical model overview

Many of the open questions in PWNe and pulsar physics appear to be strongly connected with the PW physical properties. Since the wind is cold at its basis (i.e. the particle kinetic energy is much larger than the thermal energy), no radiation is observed to come from the upstream region, that appears to the observer as an under luminous area surrounding the pulsar. As a consequence we do not have the possibility to inspect it directly. What we can do is to use the PWN emission as a diagnostic of the PW properties. To this aim a powerful tool is provided by MHD simulations coupled with non-thermal radiation modelling. One can simulate the nebular dynamics arising from different assumptions on the wind and then compute synthetic emission maps to compare with observations.

We have performed 2D MHD axisymmetric simulations with the shock capturing code ECHO [15]. The physical domain ranges from $r_{min} = 0.05$ ly to $r_{max} = 10$ ly in the radial direction, and from 0 to π in the polar one, with a suitable numerical resolution to balance the computational costs and the needed accuracy (for more details see [16, 17]). We take $v_\phi = B_r = B_\theta \equiv 0$ and the equation of state of an ideal gas with $\gamma = 4/3$, appropriate for the ultra relativistic case.

The initial conditions are chosen in order to best match the Crab Nebula's properties. The PW is injected from the inner boundary of the simulation and expands outwards, impacting the slowly expanding shell of supernova ejecta and giving rise to the relativistically hot and magnetized PWN as the system evolves.

The PW is set up according to the prescriptions of the split monopole model including a 'striped' region (namely a region in which magnetic lines of alternating polarity reconnect and the magnetisation decreases: see [16, 17] for details). In particular we assume an anisotropic energy flux for the PW, which roughly depends on space as predicted by the split monopole model:

$$F(r,\theta) = F_0 (r_0/r)^2 f(\theta), \quad f(\theta) = \frac{\alpha + (1-\alpha)\sin^2\theta}{1-(1-\alpha)/3}, \tag{2}$$

where F_0 is a constant referring to the arbitrary distance r_0 from the pulsar (set as 1 ly). The level of anisotropy is governed by the parameter α, which represents the ratio between the energy flux along the polar axis and in the equatorial plane, that must be such that $F(r, \pi/2) \gg F(r, 0)$, and thus $\alpha \ll 1$. The magnetic field, taken to be purely toroidal and $\propto r^{-1}$, has a sinusoidal dependence on the polar angle. The width of the striped region is governed by the parameter b: if $b \gg 1$ the striped region disappears, while its extent increases with decreasing b. The magnitude of the field is defined by the initial magnetization at the equator (σ_0).

The three parameters (α, b, σ_0) represent the set of free parameters of the PW model, that must be fixed comparing the computed emission properties with observations.

The broadband Crab Nebula's spectrum can be reproduced only if the contribution of two families of emitting electrons is considered: one responsible for the low energy emission (radio particles) and one for the high energy emission (optical/X-ray particles). We continuously inject particles at the TS with power law spectra for each family, $N_f(E) = K_f E^{-\gamma_f}$. The evolved distribution functions at any place in the nebula are determined by the conservation of particle number along streamlines and by the adiabatic and synchrotron losses that particles experience along their trajectory. The normalization constant K_f and the spectral index γ_f is different for radio and X-ray emitting particles. All the parameters are determined from comparison with the data (see [16, 17] for more details).

In order to compute the non-thermal emission of the nebula, 3 additional tracers have been added to the set of quantities that the code evolves [14, 16, 17]: the maximum particle energy as a function of position, ϵ_∞, namely the energy at a given location that corresponds to an infinite injection energy, the number density of non-thermal particles n and its value immediately downstream of the TS n_0. Once these are known at every point in space, the emission is computed through the standard synchrotron formulae.

5. Simulation results

The flow dynamics corresponding to the best fitting set of PW parameters (σ_0, b, α) [14, 16] allows us to reproduce the oblate shape of the TS, the observed jet-torus morphology and the correct dimensions of the nebula at its present age. In particular we assume an anisotropy parameter of $\alpha = 0.1$, thus the energy flux along the polar axis will be ten times less than at the equator. Larger contrasts are also possible in principle, but we could not investigate them with our current grid: for smaller values of α the TS tends to be very close to the pulsar along the polar axis and it easily ends up crossing the boundary of the region in which the wind is constantly reset; this fact can lead to unphysical results. Larger values of α were instead investigated in the past [11] and found unsuitable to reproduce the expected final dimensions of the nebula and the oblate shape of the TS.

However the imposed axial symmetry leads to excessive compression of the magnetic field around the polar axis, while far from the pole and from the TS the computed field is found to be well below the expected averaged value inferred from observations ($B \simeq 200\,\mu$G). Effects of this behavior are amply discussed in [16].

Our model also compares well with observations of the high energy (optical and X-ray) emission, as discussed in [14, 18].

5.1. On the origin of low energy emitting particles

So far, MHD modelling of PWNe has mainly been concerned with the properties of high energy emission, while ignoring the low energy emission. However knowledge of the origin of low energy emitting particles is of fundamental importance in the attempt to answer to some of the open questions in pulsar physics (such as the role of pulsars as antimatter factories in the Galaxy, the energetic relevance of the hadronic component of the pulsar wind and the acceleration mechanisms working at the TS [19, 20]). In fact, knowing whether radio emitting particles are fossil from previous epochs, or rather currently injected in the nebula as part of the pulsar wind, would allow one to constrain the wind Lorentz factor and the pulsar multiplicity κ, defined as the number of pairs produced in the magnetosphere for each primary electron extracted from the pulsar surface [21]. The question to assess is whether radio particles are part of the pulsar outflow, and accelerated at the TS, or if they are of different origin and accelerated somewhere else.

In the first case the inferred pair multiplicities would be generally larger than current pulsar theories are able to explain [22]: in the case of the Crab Nebula one would obtain $\kappa \sim 10^6$ for the pulsar multiplicity and $\gamma \sim 10^4$ for the wind Lorentz factor, averaged over the solid angle. On the other hand, if radio particles were of different origin, the values of these two parameters would be those inferred from high energy emission alone, namely: $\kappa \sim 10^4$ and $\Gamma \sim 10^6$ [9, 23, 21].

In [16] we studied the problem of the origin of radio particles, considering three different hypotheses. In the first scenario (case A), radio particles are considered as part of the pulsar outflow, continuously injected and accelerated at the TS with the higher energy ones. The second possibility is that they are produced somewhere else in the nebula, for instance in the thermal filaments, and then accelerated by interaction with local turbulence (case B) [24]. Finally, since radio particles are characterized by large number and long life-times against synchrotron losses, they could be of relic origin, born in a primordial outburst of the pulsar soon after the supernova explosion [25] (case C).

The synthetic emission properties at radio frequencies, in the case of the Crab Nebula, are then compared with available data. From observations we expect to find rather uniform radio emission on large spatial scales, with an ellipsoidal morphology [26]. At the same time, we also expect to find variable structures in the inner region (analogous to the optical 'wisps' [27]), changing in brightness on both short ($\Delta t \simeq 2$ months) and long ($\Delta t \simeq 3$ yr) time scales, and moving outward with mildly relativistic velocities ($v \lesssim 0.3c$).

In Fig. 1 emission maps at 1.4 GHz, for case A and B, are shown. In the left panel we show emission maps with small scale features subtracted, as in [26], for a direct comparison with that work: here the expected ellipsoidal morphology is well reproduced by the strong cylindrical symmetry given by the

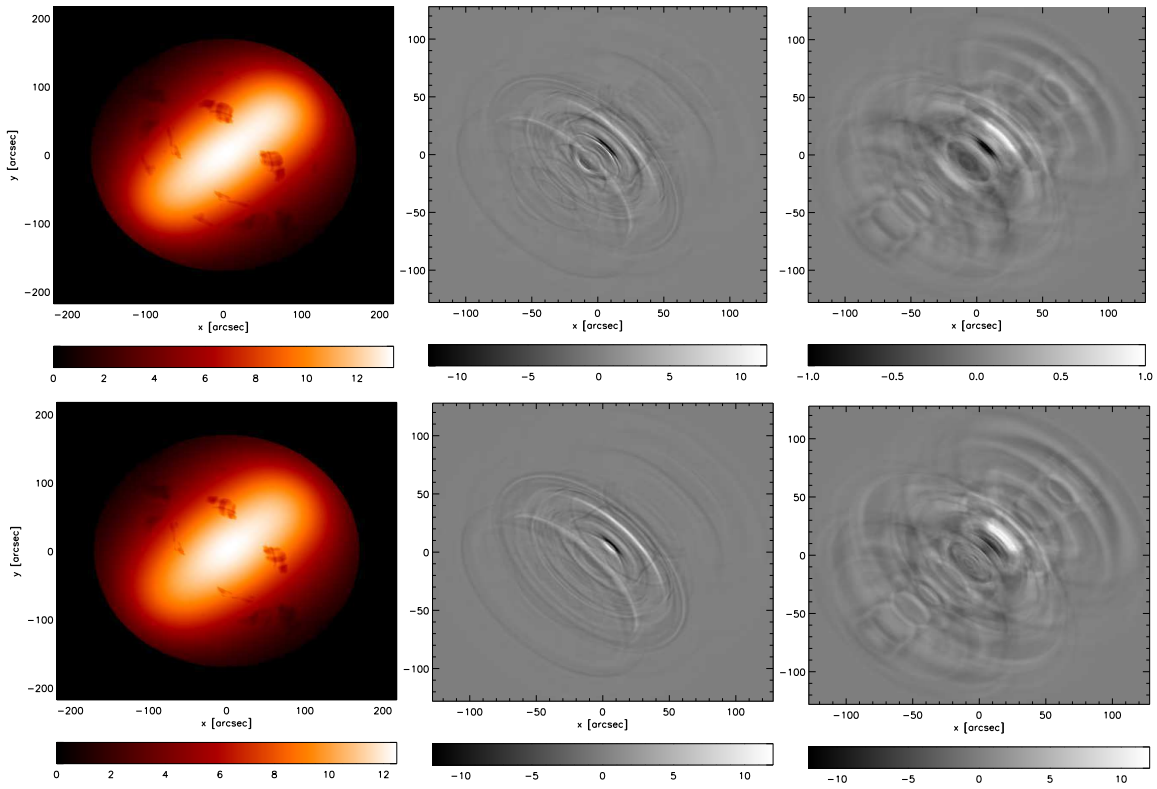

Figure 1. Radio surface brightness maps at 1.4 GHz, in units of mJy/arcsec^2. In the upper row maps for case (A) are shown, while case (B) is in the bottom. In the left panel, emission maps with the small scales subtracted are shown for both cases. In the central and rightmost panels maps of short and long time scales wisp variability are presented.

magnetic field compression around the polar axis.

In the central and right panels we show images obtained by subtracting two maps computed for epochs that are, respectively, 2 months and 3 yr apart. The maps computed under the two assumptions are basically identical. Ring-like structures, very similar to those observed at optical and X-ray frequencies, are clearly seen also at radio wavelengths, in agreement with what observed by [28] in terms of periodicity, locations and outward velocities of the so called 'radio wisps'.

The fact that results for case A and B are almost indistinguishable does not allow us to put strong constraints on the origin of radio particles. On the other hand, the important result we found is that wisps appear with the same properties under the two hypotheses. We can thus conclude that their appearance does not bear any implication on the injection site of the emitting particles, but only on the underlying flow structure: wisps simply trace the local flow and magnetic field properties, as they only arise as a combined effect of Doppler boosting and magnetic field enhancements.

The last case we considered is case C. Here we inject radio particles only at the beginning of the simulation, up to $t = t_b \ll t_{\rm PWN}$, while X-ray and optical particles are treated as in the former cases. This scenario is meant to mimic some sort of primordial outburst in which a very young pulsar would inject a wind with different properties from the current ones, namely higher multiplicity, lower Lorentz factor. What we found is that the resulting emission morphology does not compare well with observations: radio emission would mainly come from the outer region of the nebula (low energy particles advected with the flow would be confined by now to the outskirts of the nebula), while the central region would be much darker than observed. Due to the lack of radio particles in the central region of the nebula, where the magnetic field is highest and the flow is most dynamic and with the fastest speed, no wisp-like features

would be observed in this waveband. In summary, case C can be easily rejected, allowing us to conclude that radio particles cannot be described as a relic population unless a re-acceleration (and re-distribution) mechanism in the nebula is considered for $t > t_b$.

5.2. Investigating the particle acceleration mechanism

In the previous analysis we showed that within a MHD description of the flow wisps are easily accounted for as a result of regions of the nebula in which the magnetic field is strong and flow speed is high and pointing towards the observer. Wisps are seen at radio, optical and X-ray frequencies, and they are not coincident at the different wavelengths, with differences measured both in term of spatial locations and of outward velocities [27, 29]. Within the framework of MHD, the only way to account for the different properties of the wisps at different frequencies is to assume some difference in the spatial distribution of the particles that are responsible for emission in the different wavebands. An obvious difference between particles of different energies (and hence emitting in different wavebands) is the role of energy losses. However, these are not terribly important in any case in those innermost regions of the nebula, from which wisps are observed. Any other difference in the spatial distribution of the particles of different energies suggests differences in the acceleration sites. In other words, if wisps are different at radio and X-ray frequencies, the particles responsible for radio emission must have had a different history than the particles responsible for X-ray emission and the simplest explanation is that they were accelerated in different locations. Here we shall discuss how different injection scenarios reflect on different observable features of the wisps.

Essentially two acceleration mechanisms are proposed to be at work at the TS in the case of the Crab Nebula [21]: Fermi I acceleration (particles gain energy through multiple crossings of the shock front) or driven magnetic reconnection (particles are accelerated by the electric fields associated with magnetic reconnection regions). Typical spectral indices resulting from these two different processes are suitable to describe the distribution of X-ray and radio emitting particles respectively. that can account, respectively, for the high energy and radio spectral indices. The viability of the two mechanisms requires different physical conditions: Fermi I acceleration can be operative at relativistic shocks only where the magnetization is low enough (namely $\sigma < 0.001$) [30, 19], while driven magnetic reconnection requires extremely large multiplicities [31, 32, 19].

In [17] we performed a multiwavelength analysis of the wisps, considering different possibilities for the injection of particles responsible for radio, optical and X-ray wisps. Namely we define three injection scenarios: in case (1) particles are injected uniformly at the TS surface; in case (2) we define a wide equatorial zone, with $\theta \in [20^\circ, 90^\circ]$ and a narrow polar one ($\theta \in [0^\circ, 20^\circ]$); in case (3) we define a narrow equatorial zone, corresponding to the striped region of the wind ($\theta \in [70^\circ, 90^\circ]$), and a wide polar one ($\theta \in [0^\circ, 70^\circ]$). The above angular extents are expressed in the upper hemisphere, but symmetry around the equator is implicit. All the choices are considered for all three ranges of particle energies (radio, optical and X-ray emitting particles), namely, particles in each of those energy ranges can be injected in five different regions: wide or narrow polar cap, wide or narrow equatorial belt, and along the entire shock surface.

Following the analysis performed by [29], wisp profiles are extracted from synthetic intensity maps, during a period of 10 years at the end of the simulation ($t \simeq 950$ yr), and with monthly frequency. Each map is convolved with the appropriate instrumental PSFs, and intensity peaks are extracted from a 3 arcsec wide slice in the upper hemisphere, centered on the polar axis (as shown in Fig. 2). The PSFs employed are those of the instruments used for the observations considered for comparison in each frequency band: in particular we refer to the data analysed in [29, 33, 27]. The relevant observations were obtained with Chandra for the X-rays (with a FWHM=0.5″), Nord Optical Telescope (NOT) for the optical (FWHM=0.75″, as determined based on the average seeing of the period of reference), and VLA for radio frequencies (with a FWHM=1.8″)). For ease of comparison with the data in [29], only peaks with $I \geq I_{max}/3$ are taken into account, with I_{max} the maximum intensity for each map. Results are shown as plots of the radial distance of the local intensity maxima from the pulsar as a function of time

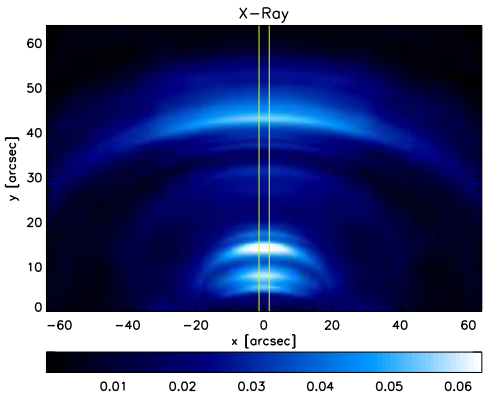

Figure 2. Upper hemisphere of an X-ray intensity map (1 keV) at t = 950 yr. Color scale is linear and in units of mJy/arcsec^2. Vertical lines near the polar axis define the slice used in the analysis of wisp profiles.

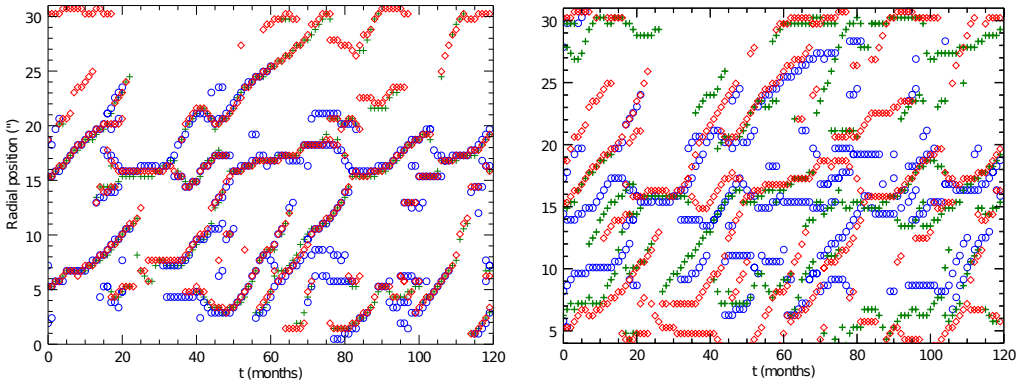

Figure 3. Radial positions of the local intensity maxima (in arcseconds) as a function of time (in months) with red diamonds identifying radio wisps (ν_r = 5 GHz), green crosses optical ones ($\nu_o = 3.75 \times 10^{14}$ Hz) and blue circles for X-rays (1 keV). On the left case (1) is shown. On the right case (3) is shown, with X-ray particles injected in the equatorial zone and radio ones injected in the complementary sector.

(in months).

Wisps behavior at radio, optical and X-ray wavelengths in the case of uniform injection (case (1)) is shown in the left panel of Fig. 3. As expected wisps are almost coincident at the different energies, with differences only due to the effect of radiation losses.

When the injection location of the different particles' populations is not coincident, the wisps are not coincident anymore at the different wavelengths. Based on our findings, in order to reproduce the X-ray wisps, which are never seen at distances from the pulsar shorter than $\sim$ 6 arcsec, the best scenario is the one in which high energy particles are injected in the narrow equatorial region of case (3) (results are shown in the right panel of Fig. 3). On the other hand, deriving strong constraints on radio particles is much more complicated: again no relevant differences are seen between uniform injection and injection in a wide sector in terms of emission properties. The only scenario that seems to be disfavoured is one in which radio particles are injected in a narrow polar cone: in this case, the variability appears to be strongly reduced.

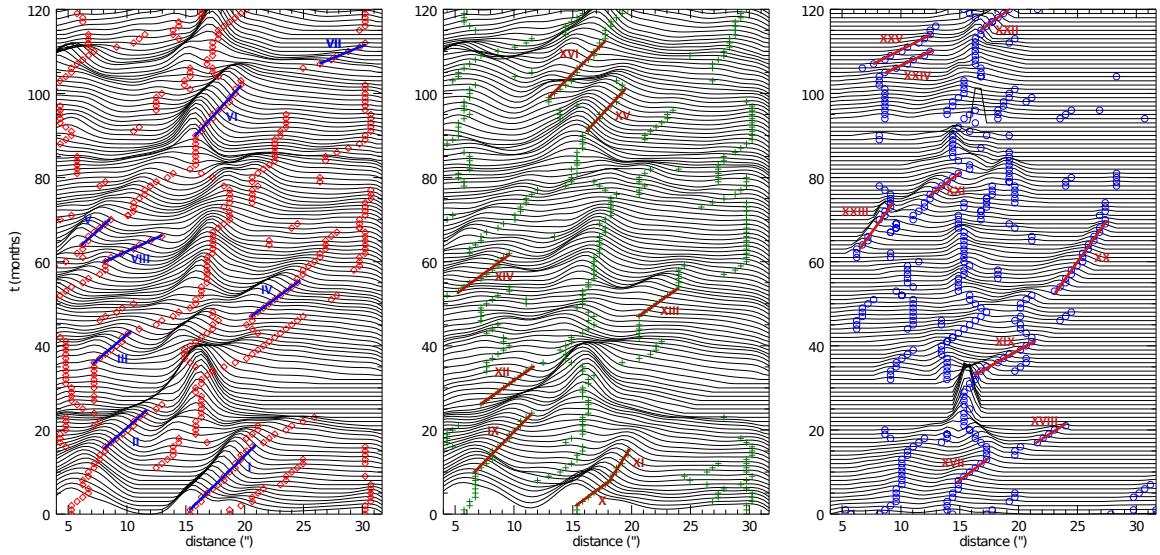

Figure 4. Stack plots with radial profiles of radiation intensity in the radio band (left panel), optical band (middle panel) and X-ray band (right panel). Results refer to case (3), with injection of X-ray particles in the narrow equatorial belt and of radio particles in the complementary wide polar region. Optical emission is contributed by both populations. Lines and Roman numerals are used to highlight the prominent structures used for evaluation of the wisp velocity.

We also computed the outward velocities of the wisps, following the time evolution of the most prominent peaks (an example is shown in Fig. 4). If the prescriptions corresponding to case (3) are followed, with radio particles injected in the wide polar cone and X-ray ones in the narrow equatorial belt, our results are in good agreement with observations: the resulting deprojected velocity is in the range $0.08c \leq v \leq 0.38c$ (to be compared with $0.1c \leq v \leq 0.4c$ from [27, 29]).

6. Summary and conclusions

Pulsar Wind Nebulae can be thought of as a relativistic version of the heliosheath, in which the solar wind is replaced by a magnetised, relativistically hot plasma. Relativistic axisymmetric MHD simulations provide a powerful tool for the investigation of the physics of this plasma, and possibly the best tool to investigate the workings of the underlying stellar source, a fast spinning, highly magnetised neutron star. While many open questions remain, the advent of relativistic MHD simulations has allowed us to answer a number of problems in recent years, and has opened a promising way to answer more.

The MHD interpretation has proven very successful at explaining the high energy morphology of PWNe: within this framework the initially puzzling jet-torus structures observed in the X-ray emission of a number of nebulae have found a straightforward interpretation as the result of the pulsar wind structure, and in particular of the anisotropy of its energy flux.

Nevertheless, this powerful tool had never been used before to investigate lower energy emission, in spite of the fact that clarifying the origin of radio particles is fundamental in order to answer many open questions in pulsar physics. We made a first attempt at a detailed study of the low energy emission properties of PWNe in the framework of 2D MHD. Our main conclusion is that the global radio emission is basically insensitive to the spatial distribution of the particles, as long as they are not pure relics. Whether they are currently part of the pulsar outflow or uniformly distributed in the nebula, the surface

brightness maps are almost identical, and also the variability of the inner regions ('radio wisps') is very similar, which proves that wisps, within the MHD framework, naturally arise from the properties of the flow.

Digging more deeply, we performed a multiwavelengths analysis of wisp properties, with the aim of constraining the history, and in particular the acceleration sites, of the emitting particles. The motivation came from observations of the nebula at different frequencies, which showed that wisps are different at radio, optical and X-rays frequencies. In an MHD description of the flow, where wisps arise as a result of the underlying flow properties, this cannot be explained, unless particles responsible for the different contributions have different acceleration sites. We considered different scenarios for the injection of particles in different energy ranges and found that properties of X-ray wisps are best reproduced if injection in a narrow belt around the pulsar rotational equator is considered. The equatorial region is presumably where the flow magnetisation is lower, if effective magnetic dissipation takes place in the striped wind. Then the mechanism responsible for the acceleration of these highest energy particles could be Fermi I, which has been proven to be very effective at relativistic shocks of low enough magnetisation [30, 19], and which naturally provide a particle spectral index close to that inferred from X-ray observations.

Constraining the radio emission properties is much more complicated: the only scenario that radio observations directly exclude is one in which low energy particles are injected in a narrow polar cone, since almost no wisps are found. But emission properties in the case of uniform injection, or injection in a wide polar or equatorial band, are basically indistinguishable.

Based on our findings a possible scenario for the particle acceleration should be the one in which high energy particles are injected in a narrow equatorial cone, where the magnetic dissipation is strong enough to allow Fermi I processes to be viable, while radio particles are injected in a wider region, where physical conditions are such that driven magnetic reconnection would be operative.

References

[1] PAMELA coll 2009 *Nature* **458** 607–609 (*Preprint* 0810.4995)
[2] AMS-02 coll 2013 *Physical Review Letters* **110** 141102
[3] Gaensler B M and Slane P O 2006 *ARA&A* **44** 17–47 (*Preprint* arXiv:astro-ph/0601081)
[4] Hester J J 2008 *ARA&A* **46** 127–155
[5] Weisskopf M C, Hester J J, Tennant A F, Elsner R F, Schulz N S, Marshall H L, Karovska M, Nichols J S, Swartz D A, Kolodziejczak J J and O'Dell S L 2000 *ApJLett* **536** L81–L84 (*Preprint* arXiv:astro-ph/0003216)
[6] Michel F C 1971 *Comments on Astrophysics and Space Physics* **3** 80
[7] Spitkovsky A 2006 *ApJLett* **648** L51–L54 (*Preprint* astro-ph/0603147)
[8] Coroniti F V 1990 *ApJ* **349** 538–545
[9] Kennel C F and Coroniti F V 1984 *ApJ* **283** 694–709
[10] Begelman M C and Li Z Y 1992 *ApJ* **397** 187–195
[11] Del Zanna L, Amato E and Bucciantini N 2004 *A&A* **421** 1063–1073 (*Preprint* astro-ph/0404355)
[12] Porth O, Komissarov S S and Keppens R 2014 *MNRAS* **438** 278–306 (*Preprint* 1310.2531)
[13] Komissarov S S 2004 *MNRAS* **350** 427–448 (*Preprint* astro-ph/0402403)
[14] Del Zanna L, Volpi D, Amato E and Bucciantini N 2006 *A&A* **453** 621–633 (*Preprint* astro-ph/0603080)
[15] Del Zanna L, Zanotti O, Bucciantini N and Londrillo P 2007 *A&A* **473** 11–30 (*Preprint* 0704.3206)
[16] Olmi B, Del Zanna L, Amato E, Bandiera R and Bucciantini N 2014 *MNRAS* **438** 1518–1525 (*Preprint* 1310.8496)
[17] Olmi B, Del Zanna L, Amato E and Bucciantini N 2015 *MNRAS* **449** 3149–3159 (*Preprint* 1502.06394)
[18] Volpi D, Del Zanna L, Amato E and Bucciantini N 2008 *A&A* **485** 337–349 (*Preprint* arXiv:0804.1323)
[19] Sironi L and Spitkovsky A 2011 *ApJ* **741** 39 (*Preprint* 1107.0977)
[20] Arons J 2012 *Space Sci. Rev.* **173** 341–367 (*Preprint* 1208.5787)
[21] Amato E 2014 *International Journal of Modern Physics Conference Series* **28** 1460160 (*Preprint* 1312.5945)
[22] Bucciantini N, Arons J and Amato E 2011 *MNRAS* **410** 381–398
[23] Gaensler B M, Arons J, Kaspi V M, Pivovaroff M J, Kawai N and Tamura K 2002 *ApJ* **569** 878–893 (*Preprint* arXiv:astro-ph/0110454)
[24] Komissarov S S 2013 *MNRAS* **428** 2459–2466 (*Preprint* 1207.3192)
[25] Atoyan A M and Aharonian F A 1996 *MNRAS* **278** 525–541
[26] Bandiera R, Neri R and Cesaroni R 2002 *A&A* **386** 1044–1054 (*Preprint* arXiv:astro-ph/0112459)

[27] Bietenholz M F, Hester J J, Frail D A and Bartel N 2004 *ApJ* **615** 794–804 (*Preprint* arXiv:astro-ph/0408061)
[28] Bietenholz M F, Frail D A and Hester J J 2001 *ApJ* **560** 254–260 (*Preprint* astro-ph/0106339)
[29] Schweizer T, Bucciantini N, Idec W, Nilsson K, Tennant A, Weisskopf M C and Zanin R 2013 *MNRAS* **433** 3325–3335 (*Preprint* 1301.1321)
[30] Spitkovsky A 2008 *ApJLett* **682** L5–L8 (*Preprint* 0802.3216)
[31] Lyubarsky Y E 2003 *MNRAS* **345** 153–160 (*Preprint* astro-ph/0306435)
[32] Lyubarsky Y and Liverts M 2008 *ApJ* **682** 1436–1442 (*Preprint* 0805.0085)
[33] Hester J J, Mori K, Burrows D, Gallagher J S, Graham J R, Halverson M, Kader A, Michel F C and Scowen P 2002 *ApJLett* **577** L49–L52